Introduction

The laser as a contact-free machining tool is continuously driving innovation to more efficient processes and new manufacturing possibilities in today's industrial production [1–3]. The growing demand of micron-sized features for the accelerating miniaturization in the sectors of electronics, optics, medical and automotive applications requires new machining processes. Ultrashort laser pulses with a pulse duration of typically less than 10 ps gained special interest as the short timescales of laser-matter interaction combined with extreme peak intensities enable new mechanisms for material modification and removal. Machining processes with ultrashort pulses are capable of generating micro structures with high quality and challenging precision in a large variety of materials [4–7]. Examples for up-to-date applications are cutting of ultrathin, hardened display glass [8] and the fabrication of drainage channels for diesel injector systems [9]. Furthermore, the manufacturing of cardiovascular stents [8] as well as selective thin film processing, e.g. electrode patterning in solar cell and display production [10, 11], is realized with ultrashort laser pulses. A further development of the processing capabilities, in particular three-dimensional structuring, is of highest relevance for future applications, especially with respect to the material classes of metals and semiconductors.

The ultrashort pulse material interaction has been subject to detailed experimental and theoretical investigations [1, 4, 12–18]. The physical mechanisms of absorption, energy redistribution, material decomposition and removal and their respective timescales are relatively well understood for ablation induced by a single pulse at a planar surface. In contrast, the laser ablation of structures with high aspect-ratio ($\geq 5:1$) at a micron size level (typically $< 100\,\mu m$ in diameter) is still a demanding task, in particular drilling of microholes. The ablation process at the hole bottom is influenced by the previously excavated hole capillary. This leads to a reduction of the drilling rate with increasing depth [19–22]. In addition, the shape formation of the hole is affected. Fig. 1 shows an example of an ultrashort pulse-drilled hole in Invar alloy with picosecond pulses.

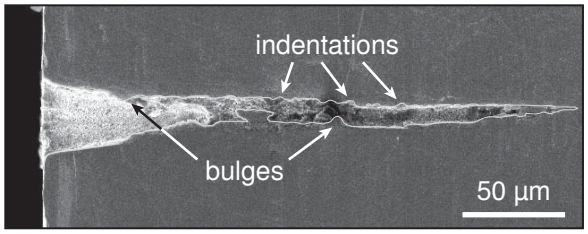

Fig. 1: Cross-section through a laser percussion-drilled microhole in Invar alloy after 50,000 laser pulses. Drilling was performed with ultrashort pulses of 8 ps duration (FWHM) at a wavelength of 1030 nm and a fluence of 10 J/cm^2.

In this cross-section, bulges and indentations cover the hole walls. Also, the hole is not straight but has a bending in the middle. The actual sizes and positions of the bulges, indentations and bendings are not reproducible even under identical drilling conditions. In some cases, the formation of multiple capillaries with different orientations can be observed in the lower part of the hole [23–25]. Although the hole entrance has a circular shape, a cross-section of the hole at a larger depth can have a nearly arbitrary shape [26, 27]. These hole shape features are typical for the laser drilling process and can be observed in different kinds of materials and under different processing conditions [21, 24, 28–30]. All in all, the benefits of ultrashort pulse ablation at the surface do not directly translate to deep microdrilling with high aspect-ratio. Therefore, profound investigations of the hole shape evolution and the mechanisms involved in the hole formation are essential for a fundamental understanding of the drilling process.

A detailed investigation of the drilling process in opaque materials, especially metals, is challenging, though. Cross-sections, as for example in fig. 1, only show the shape of a finished hole after a certain number of applied pulses. The formation of indentations, bulges and hole bendings, however, is subject to statistical variations. Hence, the specific hole shape evolution cannot be retraced by an analysis of many different holes with this technique. Direct observations of the hole formation during the drilling process have been realized with nanosecond pulses in ceramics [19, 24] and with femtosecond and sub-nanosecond pulses in diamond and polymers [21, 31]. Although these investigations currently provide the most comprehensive insights in the hole shape evolution, the involved interaction and ablation mechanisms as well as material properties differ significantly from the regime of ultrashort pulse laser drilling in metals and opaque materials. In recent years, new techniques for real-time depth monitoring in opaque materials have been developed [32, 33]. This shows the importance of detailed process investigations for the further enhancement of micro structuring with high aspect-ratio.

Several differing explanations for the peculiar evolution of the shape have been developed. This includes material inhomogeneities [21], the abrasive effect of the laser-generated plasma [19, 24], nonlinear interaction of the laser pulse with the ambient atmosphere [34–36], beam deflection by laser-induced plasma [25, 37], deposition of ablation particles inside the hole channel [26], polarization dependent reflection at the hole walls [21, 27, 38] and the influence of the hole geometry on the pulse propagation to the hole bottom [22, 39, 40]. However, the specific contribution of these possible influences on the hole shape formation are not fully understood yet.

Hence, a new approach for the analysis of the drilling process is required. In this work, an in-situ observation of drilling in an opaque material is realized for the first time. The principle is based on the use of crystalline silicon as the sample material. It is transparent for laser wavelengths above the band edge at ca. 1100 nm [41] and opaque for lower wavelengths, including the typical ultrashort pulse laser systems for material processing, i.e. wavelengths of 1030 nm, 800 nm and 515 nm. Furthermore, the ablation behavior of silicon is similar to a metal at these wavelengths in the ultrashort pulse regime [15, 42, 43] and drillings with high aspect-ratio are possible [22]. It is therefore used here as a model system for drilling of semiconductors as well as the industrially relevant material class of metals. During drilling, the sample is illuminated by a second laser with a wavelength of 1060 nm. At this wavelength, silicon is nearly transparent but a standard silicon-based camera sensor can still produce a high-contrast image of the hole silhouette.

This study concentrates on the technique of percussion drilling, where the position of the laser focus stays constant during the complete drilling procedure, usually at the sample surface [44]. In this case, the diameter of the resulting hole is similar to the size of the focal spot. Therefore, the most distinct influence of the hole capillary on the further hole formation and depth evolution can be expected.

The present work pursues a systematic investigation of the effect of the laser and process parameters on the hole shape evolution including the pulse energy, fluence, pulse duration, wavelength and focus position. Moreover, the role of particle debris inside the hole channel, the interaction of subsequent laser pulses with previously ablated material inside the hole, the expansion of the plasma plume and the light propagation inside the hole capillary are studied as possible reasons for the special hole shape formation.

Structure of this Thesis

This thesis is organized in five chapters.

Chapter 1 gives a short review of the fundamental physical processes of laser ablation with short and ultrashort laser pulses.

Chapter 2 then summarizes the state-of-the-art experimental techniques for the investigation of laser deep drilling and their specific advantages and limitations. This is followed by a review of the current state of knowledge on the laser drilling process.

Chapter 3 presents the experimental realization of the in-situ drilling observation with silicon as the sample material. This technique is then used in different configurations to investigate the influence of laser and processing conditions on the hole shape evolution.

Chapter 4 covers the results of hole shape evolution and depth development by in-situ imaging of the percussion drilling process. Different laser parameters, e.g. pulse energy, wavelength, pulse duration, as well as different processing conditions, e.g. applied fluence and focus position, are under investigation. A common, general description of the hole formation process is developed.

Chapter 5 focuses on the physical mechanisms of the hole shape formation, especially the reasons for the formation of special shape features, i.e. bending, bulges and indentations. The effect of the ablation particles, the interaction of consecutive pulses, the expansion of the laser-generated plasma and the pulse propagation through the hole capillary are studied in detail.

Finally, this thesis is completed with a conclusion conveying the essential findings and an outlook of possible methods to enhance the drilling precision and further investigations for an advanced understanding of the hole formation process in ultrashort pulse laser deep drilling.

1 Fundamentals of Short and Ultrashort Pulse Laser Ablation

The laser ablation process is characterized by the physical mechanisms of absorption, energy diffusion, material decomposition and expansion of the material vapor. This chapter gives a short review of the laser-matter interaction by short and ultrashort pulses and the respective timescales of the ablation mechanisms. The following discussion is mostly based on experimental and theoretical studies of the ablation behavior of metals and semiconductors.

1.1 Energy Absorption and Redistribution

The energy of the laser pulse is first absorbed by the electrons [45], e.g. by free-free transition of the electrons in the conduction band of a metal. The heavy ions of the lattice cannot follow the high-frequency oscillation of the incident electromagnetic field. Thermalization within the electron system takes place rapidly, typically on a femtosecond timescale [46], which leads to a thermal energy distribution. Therefore, it is usually assumed that the energy of the electron system can be characterized by a temperature [35, 47]. The energy transfer from the electrons to the lattice is mediated by electron-phonon coupling [48] which typically takes place on a timescale of 1 ps to 100 ps [14, 49, 50]. Consequently, the temperature of the lattice can be different from the electron temperature and needs to be characterized separately [47], especially for pulses with a duration equal to or even shorter than this coupling time. The evolution of the electron temperature T_{el} and the lattice temperature T_{lat} can be described by the Two-Temperature-Model [47] according to

$$\begin{aligned} C_{\mathrm{el}}\frac{\partial T_{\mathrm{el}}}{\partial t} &= \nabla\cdot\left(\kappa_{\mathrm{el}}\nabla T_{\mathrm{el}}\right) - G\cdot\left(T_{\mathrm{el}}-T_{\mathrm{lat}}\right)+Q, \\ C_{\mathrm{lat}}\frac{\partial T_{\mathrm{lat}}}{\partial t} &= \nabla\cdot\left(\kappa_{\mathrm{lat}}\nabla T_{\mathrm{lat}}\right) + G\cdot\left(T_{\mathrm{el}}-T_{\mathrm{lat}}\right). \end{aligned} \tag{1.1}$$

C_{el} and C_{lat} denote the electron and lattice heat capacities and κ_{el}, κ_{lat} the respective thermal conductivities. G is the electron-phonon coupling coefficient. In general, all these parameters are temperature dependent themselves. The heat source Q can be derived from the absorption of the laser pulse by the Bouguer-Lambert-Beer law [1]. For a laser pulse with intensity I and perpendicular incidence on the surface in z-direction, it is given by [4]

$$Q = \alpha\left(1-R\right)I\cdot\exp\left[-\alpha z\right] \tag{1.2}$$

in which α is the absorption coefficient and R the surface reflectivity of the material. This means, the pulse energy is initially deposited in a layer with a characteristic thickness of $l_\alpha = \alpha^{-1}$ which is the so-called optical penetration depth. For metals, this is typically a thin surface layer with a few nanometer thickness [1, 51].

For pulses with high peak power, absorption can be induced in otherwise transparent media (e.g. dielectrics) due to the generation of free electrons from multiphoton absorption or field ionization [12, 14]. The trailing part of the pulse is then absorbed by these free electrons similar to the situation in a metal. The further process of energy transfer can be described with the Two-Temperature-Model. In this case, the effect of the changing free electron density on the thermal (C, κ, γ) and optical properties (R, α) has to be considered as well [52, 53].

To illustrate the typical evolution of the electron and lattice temperature, fig. 1.1 shows a numerical solution of the Two-Temperature-Model according to equation 1.1. In this example, a copper sample is irradiated by a pulse with a Gaussian temporal profile and a duration of 1 ps. The absorbed fluence, i.e. the pulse energy per irradiated area, is $F_{\mathrm{abs}} = (1-R)\cdot F = 0.2\,\mathrm{J/cm^2}$. Temperature dependent values of the electron heat capacity and the electron thermal conductivity are considered in the model. A detailed description can be found in appendix A, p. 101. The simplified simulation here does not account for changes of the material phase, i.e. melting and evaporation, and removal of material. Nevertheless, the temperature represents the energy distribution within the system.

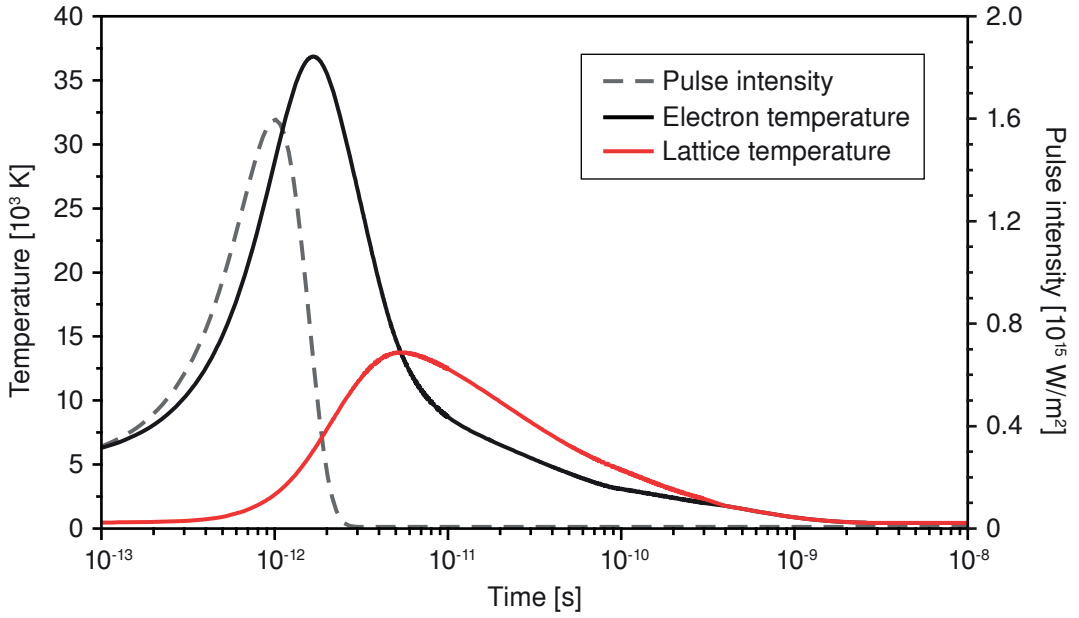

Fig. 1.1: Simulated electron and lattice temperature evolution in copper according to the Two-Temperature-Model. The temporal profile of the pulse intensity is given as a dashed line for reference. The pulse duration is 1 ps and the entire absorbed fluence adds up to $F_{abs} = (1-R) \cdot F = 0.2\,\mathrm{J/cm^2}$.

At the beginning of the laser pulse, the temperate of the electrons rises rapidly with the increasing pulse intensity, i.e. mainly in the first picosecond. The maximum electron temperature reaches several ten thousand Kelvin due to the low electron heat capacity. The energy transfer from the electrons to the lattice is delayed with a characteristic electron-phonon coupling time $\tau_{\text{el-ph}}$. This coupling time can be defined from the time constants of electron cooling $\tau_{\text{el}} = C_{\text{el}}/G$ and lattice heating $\tau_{\text{lat}} = C_{\text{lat}}/G$ as [1]

$$\tau_{\text{el-ph}} = \left[\frac{1}{\tau_{\text{el}}} + \frac{1}{\tau_{\text{lat}}}\right]^{-1} = \frac{C_{\text{el}} \cdot C_{\text{lat}}}{G \cdot \left(C_{\text{el}} + C_{\text{lat}}\right)}. \tag{1.3}$$

In the example in fig. 1.1, $\tau_{\text{el-ph}}$ is longer than the pulse duration and the maximum lattice temperature is reached only after several picoseconds, i.e. significantly after the end of the laser pulse. Typical values of the electron-phonon coupling coefficient, heat capacities and the resulting coupling time $\tau_{\text{el-ph}}$ for different metals are summarized in tab. 1.1. For metals, the characteristic coupling time $\tau_{\text{el-ph}}$ is generally in the order of several picoseconds. If the pulse duration is shorter than the electron-phonon coupling time, heating of the lattice as well as heat diffusion occurs after the irradiation and

Tab. 1.1: Electron-phonon coupling time for aluminum, copper, iron and gold at an assumed electron temperature of 10,000 K [54].

		Al	Cu	Fe	Au
G	$[10^{17}\,\mathrm{W/m^3K}]$	5.7	1.0	2.4	0.2
C_{lat}	$[10^{6}\,\mathrm{J/m^3K}]$	2.4	3.5	3.5	2.5
C_{el}	$[10^{6}\,\mathrm{J/m^3K}]$	1.4	1.0	5.0	0.7
$\tau_{\text{el-ph}}$	$[\mathrm{ps}]$	1.5	7.6	8.6	26.3

is therefore mainly determined by the material properties. Such a pulse duration is referred to as ultrashort, which typically means 10 ps or less. In this case, heat diffusion is limited to the lowest possible amount for the specific material and the energy stays confined within the irradiated area [15]. Equalization of electron and lattice temperature then occurs after several cycles of $\tau_{\text{el-ph}}$. Afterwards the electron and lattice subsystems can be described by one common temperature, see e.g. the time domain after 300 ps in fig. 1.1. The ablation depth can be calculated from the Two-Temperature-Model simulation either by considering phase transitions in the model or by comparison of the energy content within the electron and lattice systems to the necessary enthalpy for melting and evaporation. In the ultrashort pulse regime, the amount of removed material is in general independent of the actual pulse duration and primarily determined by the applied fluence [55].

For pulses with a duration longer than $\tau_{\text{el-ph}}$, especially longer than several hundred picoseconds, heating of the electron subsystem is comparably slow and the energy transfer to the lattice occurs almost instantaneously. Consequently, the complete energy distribution can be described by a One-Temperature-Model [4]. In this case, significant thermal diffusion already occurs during irradiation, especially for materials with high thermal conductivity like metals. The incident energy spreads into the surrounding material with a characteristic thermal diffusion length $l_{\mathrm{th}} \approx \sqrt{\frac{\kappa}{C} \cdot \tau_{\mathrm{pulse}}}$, which depends on the thermal conductivity κ and the heat capacity C. It increases with the pulse duration τ_{pulse} and can reach 1 µm to 10 µm for a 100 ns-pulse [17]. Therefore, the heat affected zone is larger than the irradiated area for long laser pulses and the ablation threshold as well as the ablation depth strongly depend on the actual pulse duration [4, 56].

In general, the Two-Temperature-Model has been successfully employed for the theoretical discussion and numerical calculation of the ablation threshold, the ablation depth, the melt layer thickness and the heat affected zone [2, 4, 35, 50, 52, 55, 57–62].

1.2 Material Removal Processes

For ultrashort laser pulses, the process of material removal takes place in two stages. In a first step, the high temperatures of the electrons and the lattice cause the thermionic emission of electrons in combination with sublimation and direct transition of the solid to the plasma state [17, 47, 63–65]. The ablation products are therefore electrons, ions and atoms or molecules, which are emitted from the surface on a nanosecond timescale or faster [13, 15, 66].

In a second step, the rapid isochore heating of the lattice results in a superheated layer which is subject to high thermoelastic pressure [1, 67, 68]. The relaxation of this stress leads to the amorphization of the surface layer and desorption from the surface. Simultaneously, nucleation of bubbles and larger voids takes place below the surface. The coalescence of these voids creates a foam-like structure with the amorphous layer on top, which separates from the solid [18, 67, 69–72]. This way of fracturing of the solid, also referred to as spallation, causes ablation in the form of clustered atoms as well as nanoparticles [73–77]. For higher absorbed energy densities, the spallation process turns into rapid melting and direct heating of the solid above a critical temperature for phase separation which is approximately 6000 K for metals like iron, aluminum and copper [1, 18, 65]. A decrease in pressure due to expansion initiates massive homogeneous nucleation followed by a breakdown of the liquid into a liquid-gas mixture with explosive expansion [70, 78]. This so-called phase explosion generates vapor and plasma as well as liquid droplets [40, 63]. This second step of ablation occurs after a delay of several tens of nanoseconds [65]. The fraction of material that is removed by spallation and phase explosion in comparison to the direct transition to plasma in the first step depends on the total absorbed fluence and pulse duration. It is lowest for a fluence close to the ablation threshold, whereas ablation at a high fluence occurs mainly via phase explosion [17, 65]. The material removal processes of ultrashort pulses are independent from the exact interatomic potential [71, 79–81] and therefore similar for different material classes, e.g. metals, semiconductors or dielectrics.

A part of the absorbed pulse energy does not contribute to ablation [35]. Hence, the solid surrounding the ablation region is heated and even melted without ablation. Nevertheless, for ultrashort pulses, the thickness of the melt layer is typically below 1 µm [35]. Its maximum thickness is reached after a few tens of nanoseconds and complete resolidification ends after several tens to hundreds of nanoseconds. The timescales of these thermal processes are determined mainly by the material properties in case of ultrashort pulses, when energy deposition is faster than the material response.

For long pulses with nanosecond duration or longer, the material reaches the critical temperature for phase explosion only at high incident energy densities [82, 83]. Otherwise, especially for pulses in the microsecond and millisecond regime, "normal" boiling with heterogeneous nucleation leads to gradual evaporation [1]. This process is accompanied by significant thermal diffusion and pronounced generation of melt, see also the thermal penetration depth l_{th} for long pulses as discussed above. The characteristic times for vaporization and resolidification increase with the pulse duration in combination with a significant increase of the melt layer thickness which can considerably exceed 1 µm [35]. In addition, the recoil pressure from the material vapor leads to the expulsion of melt at the rim of the ablation crater [2]. Melt deposition around and inside the ablation area distort the geometry and also create burr. For ultrashort laser pulses, low melt layer thickness and fast solidification substantially reduce the formation of burr [5].

1.3 Material Vapor and Plasma

The decomposition of the material during the ablation process generates a spherical shock wave in the atmosphere surrounding the laser spot [1, 2]. This shock wave is similar for short and ultrashort laser pulses. The material vapor cloud expands behind the shock wave. For pulses in the picosecond regime and longer, a symmetric shape of the vapor plume can be observed while sub-picosecond pulses create a turbulent vapor flow [84]. For a time span of several tens of microseconds, the vapor expands gradually and separates from the surface. Afterwards, typically on a timescale of 100 µs, a breakup of the plume is observed in combination with the formation of complex flow patterns including swirls [15, 84]. These patterns show large statistical variations, even if ablation is repeated under identical irradiation conditions.